University of Arkansas, Fayetteville

ScholarWorks@UARK

Theses and Dissertations

5-2020

Characterization of Avidin and Case9 Single Protein Molecules by a Solid-state Nanopore Device

Haopeng Li
University of Arkansas, Fayetteville

Follow this and additional works at: https://scholarworks.uark.edu/etd

Part of the Biochemistry Commons, Biophysics Commons, and the Nanoscience and Nanotechnology Commons

Characterization of Avidin and Case9 Single Protein Molecules by a Solid-state Nanopore Device

A thesis submitted in partial fulfillment
of the requirements for the degree of
Master of Science in Cell and Molecular Biology

by

Haopeng Li
University of Arkansas
Bachelor of Arts in Biology, 2016

May 2020
University of Arkansas

This thesis is approved for recommendation to the Graduate Council.

_____
Jiali Li, Ph.D.
Thesis Director

_____
Timothy Alan Kral, Ph.D.
Committee Member

_____
Suresh Thallapuranam, Ph.D.
Committee Member

Abstract

The shape and charge of a protein play significant roles in protein dynamics in the biological system of humans and animals. Characterizing and quantifying the shape and charge of a protein at the single-molecule level remains a challenge. Solid-state nanopores made of silicon nitride (SiN_x) have emerged as novel platforms for biosensing such as diagnostics for single-molecule detection and DNA sequencing. SSN detection is based on measuring the variations in ionic conductance as charged biomolecules translocate through nanometer-sized channels driven by an external voltage applied across the membrane. In this paper, we observe the translocation of asymmetric cylindrical structure CRISPR-Cas9 protein and symmetric cylindrical structure Avidin protein driven by an electric field through the solid-state nanopore. We also observe how glycerol impacts on the time durations and current blockage amplitudes produced by the translocation of two proteins in nanopore by using different glycerol concentrations.

Contents

Introduction

The primary structure of a protein which is an amino acid is the basic form and is generally considered to be inactive. When the linear amino acid sequence folds into a three-dimensional structure, it becomes an active protein and plays an important role in biological systems. Fully folded proteins have a certain shape and function in all aspects of human life such as regulating the metabolism and immune system. Protein characterization which includes protein size and shape measurements is essential to understand its functioning mechanisms in the human body. As a part of protein characterization, detecting the shape of a protein could provide the three-dimensional structure data to help researchers monitor the dynamics of the proteins. The traditional methods for protein characterization such as scanning electron microscopy (SEM)[1], Fluorescence resonance energy transfer (FRET)[2], and laser-induced fluorescence (LIF)[3]. Likewise, biomechanical tools are widely applied in recent decades, such as magnetic tweezers[4], optic tweezers[5,] and atomic force microscopy (AFM)[6]. Although these methods are reliable and useful, the disadvantages are also evident. Pretreatments of samples are required and it may impact the native proteins' properties. Convoluted experimental procedures are challenging for researchers. Expensive and intricate equipment setup and materials could restrict its development.

Nanopores are classified into three classes: (1) Synthetic nanopores fabricated in solid substrates, such as Si_3N_4; (2) Biological pores embedded in a lipid bilayer and (3) Hybrid of biological and synthetic nanopores. They all have their advantages and disadvantages.

The substrate of choice for all biological pores in planar lipid membranes, polymer membranes or liposomes placed inside an electrochemical chamber. Standard molecular biology techniques can produce and purification various channel proteins on a large scale. It is safe to say that the

channel pores from different purified batches are homogeneous. Moreover, it is possible to

employ site-directed mutagenesis to explicitly fabricate the channel pores because of several

proteins' crystal structure[7]. α-Hemolysin channel, MspA channel MspA (Mycobacterium

smegmatis porin A) and Phi29 Connector channel are three well studied biological pores. Human

pathogen *Staphylococcus aureus* secrets an exotoxin called α-Hemolysin. It is a heptameric

transmembrane pore that resembles the mushroom shape, consisting of a vestibule connected to a

transmembrane β-barrel[7]. The narrowest part of the pore is at the vestibule which has a diameter

of around 1.4 nm. The α-Hemolysin has demonstrated significant potential in the random

detection of various analytes. However, the limitation is also evident, because of the pore size,

the use of the α-Hemolysin channel is restricted to the translocation of small analytes such as

ssDNA. The procedure of α-hemolysin channel proteins inserting into the lipid bilayer is

spontaneous. It is thermally stable, functioning at temperatures near 100°C, it can also endure a

wide pH range from 2-12 while retaining the original structure. The β-barrel portion of the α-

hemolysin channel is particularly attractive to genetic engineer and chemist due to it's obedient

to rational modifications for introducing specific binding elements.

MspA channel is an octameric channel pore found in *Mycobacterium smegmatis* porin A which

resembles a funnel shape. It functions as a tunnel for the transportation of water-soluble

molecules across bacterial cell membranes. The Neiderweis lab demonstrated the crystal

structure that reveals the single narrowest part is around 1.2 nm wide and 0.6 nm long[8]. So many

experiments are encouraged by this fundamental but essential discovery. Like α-hemolysin, the

formation of a nanopore consists of MspA channels inserting into a planar bilayer is also

spontaneous[9]. MspA is more robust because it can maintain channel-forming activity after

incubation at 80°C in presence of 2% SDS or even extraction at 100°C for 30 min at any pH

from 0 to 14[9]. Mutagenesis on specific sites can be conducted by chemical fabrication on mutant channels thanks to the discovered crystal structure[8].

Phi29 connector channel is the first channel that is neither a membrane protein nor an ion channel inserted into a lipid bilayer[10]. The DNA-packaging nanomotor of bacterial virus phi29 contains a refined elaborate channel composed of twelve copies of the protein gp10, which surrounds to form a dodecamer channel[11,12], and this channel functions as a route for the translocation of double-stranded DNA. The anchoring and insertion of the connector with the viral capsid are mediated through protein-protein interactions[12]. Some robust traits followed by extremely firm, accurate and sensitive conductance signatures are generated from the resulting system when DNA or ions translocate through the channel after the insertion of the connector into the lipid bilayer, as revealed by single-channel conductance measurements[13]. However, the insertion of the connector into the lipid bilayer is not spontaneous. Artificial intervene is required, the connector is reconstituted into lipid vesicles during the rehydration, followed by vesicle fusion with a planar bilayer[13]. The conductance of each pore remains nearly identical, and it is completely linear with respect to the applied voltage. The connector channel is also steady under a wide range of experimental conditions such as extreme pH and high salt solution[14]. The one factor that the phi29 system exceeds the other two systems is its larger channel size allowing all kinds of molecules such as dsDNA, dsDNA, small proteins and peptides. The advantages of larger pore size also permit more convenient channel modifications such as generating a sensitive detection region for achieving single-nucleotide resolution or detection and diagnostic on conjugation or insertion of chemical groups[15].

As a versatile alternative to biological nanopores, solid-state nanopores have their unique advantages including definitive geometries and dimensions, mechanical robustness, simple

3

modifications and compatibility with various electronic or optical measurement techniques. Various ranges from one to hundreds of nanometers of diameter in solid-state nanopore can be precisely controlled by the experimental requirement. Generally, solid-state nanopores such as SiN is a dielectric material, it exhibits exceptional thermal and chemical stability over lipid membrane[6]. However, their stability relies on the method used to fabricate these pores[16]. Not all solid-state nanopores are perfect, but the solid-state nanopore is still better than its biological opponents due to its unique electrical properties. In recent decades, solid-state nanopore has encouraged so many applications, such as detecting protein interactions[17]. Meanwhile, different kinds of fabrication methods are developed as well such as ion beam sculpting[18].

Silicon-based substrates like silicon nitride (SiN) and silicon dioxide (SiO_2) have been favored as a substrate over the years due to its low mechanical stress and exceptional chemical resistance. High temperatures and low-pressure chemical vapor deposition are frequently used to fabricate silicon substrates. Standard wet-etching (KOH) techniques and photolithography are employed to create 100-μm × 100-μm window on the top side, then focus electron beam (FEB) or focus ion beam (FIB) is applied to sputter atoms away from the SiN membrane to drill a hole in the center. Precise controlling the diameter of the nanopore is always guaranteed. Conventional SiN membranes are typically 20 to 30 nm thick. The high salt solution is needed to screen the negatively charged surface of SiO2 or SiN[19]. Linear I-V relationship is observed even at high voltages. SiN pores were primarily used in DNA translocation studies, but more and more applications of SiN pores on different biomolecules are demonstrated[48]. The graphene sheet is a 2D sheet of carbon atoms. 2-25 nm diameter pores have been fabricated in suspended graphene films, composed of one or two layers of carbon atoms and dsDNA was translocated through the pores[67]. DNA sequencing is especially attracted by graphene nanopores because of its

exceptional electrical, thermal and mechanical properties. Interestedly, the ionic current signal measured will be convolution because of a few nucleotides twisting in or around the pore, therefore it possesses the higher spatial resolution compared to other thicker solid-state nanopore which accommodates significantly more DNA[68]. Moreover, a lateral voltage across the nanopore membranes is permitted in graphene nanopore[69]. Theoretically, it is possible to measure the lateral tunneling using nanofabricated graphene electrodes. Therefore the current in the tunnel across the nanopore is associated with the individual molecules which go through the nanopore, the resolution of nanopore biomolecule can be greatly improved[70,15].

DNA sequencing was the first popular research area. In 2004, the National Human Genome Research Institute launched the "$1000 genome project" to expand next-generation sequencing (NGS) techniques, such that a human genome can be sequenced rapidly for less than $1000. Schadt.et.al has categorized the NSG into three generations[20]. First-generation sequencing based on Sanger's approach: has a read length of 400-900 bp with 99.9% accuracy at a cost of $2400 per million base[21]. The second-generation sequencing techniques are based on the amplification of target DNA and large numbers of parallel chips. Although 2nd generation sequencing brings down the cost to less than $1000, the DNA read length is compromised to a few hundred bases and it takes longer time[22]. New technologies are developing rapidly in order to overcome the limitations of previous generations. Those techniques that focus on the single-molecule level are known as third-generation techniques such as Nanopore sequencing[23], single-molecule motion[24], molecular force spectrometry[25], sequencing by tip-enhanced Raman scattering[26]. These techniques share a common feature which is no requirement for complicated sample preparation procedure. Nanopore technology has more practical benefits such as uncomplicated sample preparation, label-free or chemical modification-free; real-time detection and result[27]. After a

tremendous amount of progress made on nanopore sensor as a next-generation detection method to detect and monitor multiple properties of DNA molecules in their different environments by measuring the ionic current blockages in voltage biased nanofabricated pores[28-32], detecting molecules with a size comparable or larger than DNA, such as short peptides, small proteins, as well as protein and any biochemical species have been investigated in recent years[33-35]. Information on the proteins can be obtained by analyzing the data. Some brilliant results are found such as Pradeep Waduge's discovery on the correlation between the shape of the current signal amplitude distributions and the protein fluctuation as obtained from molecular dynamics simulations[36]. Gautam V. Soni observed a systematic dependence of the conductance blockade and translocation time on the molecular weight of the nucleosomal[37]. The shape and volume of single protein molecules are estimated by Erik C. Yusko by analyzing individual resistive pulses current values[38].

Nanopore sensor detection can be summarized as the combination of ion channel[39] and resistive pulse technique[40]. A solid-state nanopore is a nanometer-sized hole that is etched in a thin silicon nitride (Si_3N_4) membrane and it is placed between two isolated chambers (made by PDMS). One silver/silver chloride electrode is placed in each of the two chambers to provide voltage. When voltage is applied across the nanopore in a salt solution, the electric field inside drives the ions in the salt solution to flow through the open nanopore generating an ionic current and the open pore current I_0 (baseline current) is established and detected by a patch-clamp amplifier. The baseline current is determined by the pore geometry and solution conductivity σ. A fundamental example would be a cylindrical geometry, the relationship between I_0 and applied voltage (V) can be predicted using Ohms law[41]:

$$I_0 = \frac{V\sigma\pi r^2}{H} \qquad (1)$$

Respectively, r and H are radius and thickness of the nanopore. A basic set up of a solid-state-nanopore translocation experiment is shown in Fig 1(b). Upon addition of charged biomolecules in the cis chamber, molecules will diffuse to the pore and translocate through the pore driven by the electric field, thus temporarily blocking the passage of ions that leads to a decrease in the open pore current, this simple transient current blockage event can be recorded and measured. The Current drop is represented as ΔI_b. In this case, we use equation (2) to estimate the excluded volume of protein[42]:

$$\Delta I_b = \frac{\gamma AV}{\rho(l_p + 1.6r_p)^2} \qquad (2)$$

where γ is the shape factor of the protein, V is the applied voltage across the nanopore, H the effective thickness of the nanopore, and A the volume of the translocating molecule. ρ (Ω m) represents the resistivity of the electrolyte, l_p is the length of the pore and r_p the radius of the nanopore[43].

Briefly, the relationship between normalized resistive pulse magnitude $\Delta I/I_0$, and the volume of the associated translocating particle traces back to Maxwell's derivation[44,45,66]

$$\frac{\Delta I}{I_o} = -\frac{4A\,\gamma}{\pi d_p^2(l_p + 0.8d_p)} \qquad (3)$$

Where A is the volume of the particle, γ is the particle's electrical shape factor ($\gamma = 1.5$ for perfect spheres), d_p is the diameter of the pore, l_p is the length of the pore.

Nanopore concentrates on a single molecular species at a time during sequencing, with the spatial resolution within the molecule being the main focus[46]. The translocation velocity and molecule capture rate can be optimized by either controlling the nanopore electroosmotic speed[47] through different solution properties, such as salt concentration, temperature, viscosity (which

modifies the electric potential bias across the nanopore)[49]. On the other side, it is challenging to develop a general platform to distinguish a broad range of molecules with different electrical and physical properties in terms of multiple biomolecules such as protein detection for diagnostic applications. A method to effectively snare proteins with different size/charge ratios in nanopores in the same solution conditions is desired. Recently molecular dynamics simulations have demonstrated that the nanopore ionic current can be potentially used to characterize the conformation changes of a protein inside the nanopore with high resolution[49,50]. Pioneering works have validated the theoretical observations that nanopore ionic current can be potentially used to characterize the conformation changes of a protein inside the nanopore[51]. Although the folding and unfolding of protein play a crucial role in human physiology, the structure and three-dimensional shape of the protein are as significant as its dynamic role in human metabolism. The successful characterization of the unlabeled and folded protein in aqueous environments at the single-molecule level was reported[52].

A recent study where Avidin molecules are monitored passing through ClyA, a biological dodecamer nanopore provided fascinating results[53]. We are curious to compare how Avidin and Cas9 protein will perform through the solid-state nanopore in different salt and glycerol concentration. The nanopore made of silicon nitride[54] is employed to provide its particular strengths such as high sensitivity, label-free, chemical, and thermal robustness[55].

Avidin is a tetrameric biotin-binding protein found in the oviduct and deposited in the albumen fraction of eggs, many studies been conducted on avidin due to the remarkable ligand-binding activity and unusual solution stability[56]. Avidin has four identical subunits consisting of 128 amino acids with a total size of 67kDa and a high isoelectric point of approximately 9.5[57,58], and its dimension of 7.1 nm $\times$ 6.7 nm $\times$ 5.5 nm is well comprehended from X-ray studies[59,60].

Clustered Regularly Interspaced Short Palindromic Repeats (CRISPR) and its CRISPR-associated (Cas9 protein) which consist of 1376 amino acids and has a size of 160 kDa with the dimensions of 15 nm $\times$ 20 nm $\times$ 9 nm and the size of 160 kDa from crystal structures[61] are also employed due to its enormous popularity in genetic engineering, the Cas9 protein can bind to the target DNA sequence through guide RNA (gRNA)[62]. However, unlike highly negatively charged DNA molecules whose total charge is proportional to the number of bases, protein molecules are independent of their number of residues, sequence, or size. But can be charged by applying pH that is higher or lower than proteins' isoelectric point. The irregular shape and charge distribution will require a different strategy to detect proteins.

In this paper, we report that the attempted characterization of spherical protein avidin and non-spherical Cas9 protein by the ionic current through the solid-state nanopore and how viscosity and salt solution affect the translocation. The study performed here can be potentially used to prove that nanopore identification of single protein molecules in real-time is qualified to be applied in the real world. It might ultimately become a feasible biochemical and clinical detection method for an individual's proteome and single-molecule sorting in the future.
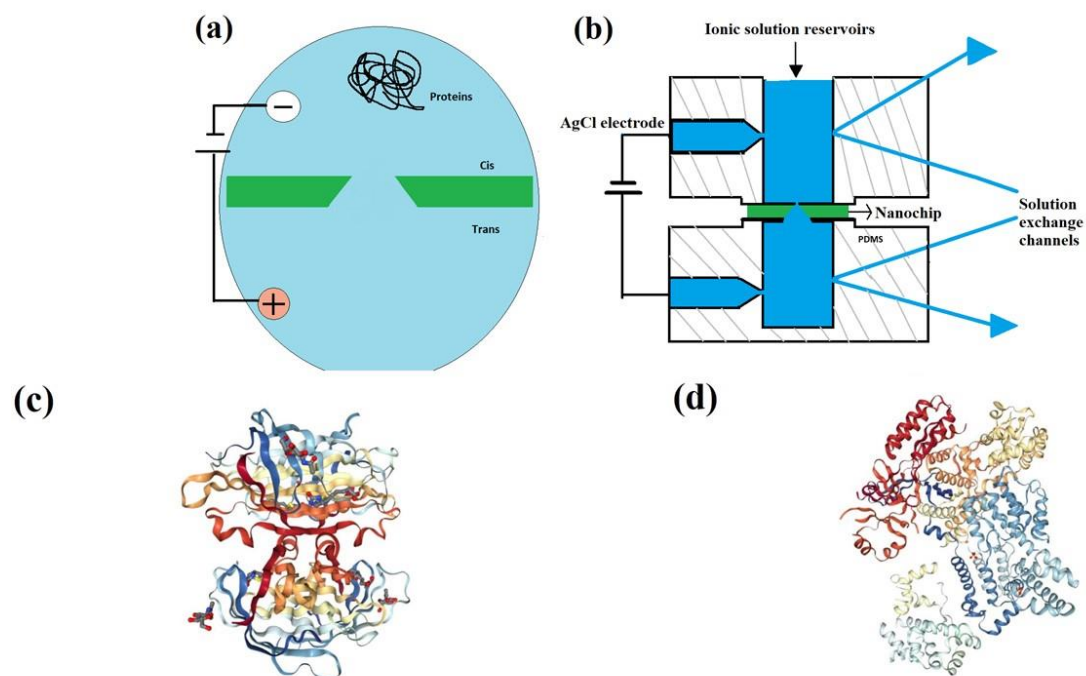
Figure 1: (a) A molecule translocating through a nanopore is schematically illustrated. (b). Experimental setup for single-molecule measurements with nanochip between the two chambers. (c) A 3D representation of Avidin (2AVI pdf file). (d) A 3D representation of S. pyogenes Cas9 (4CMP pdf file).

Experiment Setup

Nanopore chips are cleaned by sulfuric acid and hydrogen peroxide in a 3:1 ratio mixed solution

at 90ºC for 30 minutes, then rinsed with deionized water for 30 minutes, and finally soaked

overnight in deionized water. A chip is aligned between two ~80 μL PDMS chambers. These

chambers are filled electrolyte which contains 1.6 M NaCl, 20% glycerol and 150 mM Tris

buffer solution at pH 7.5. 1.6 M NaCl solution is filtered with a 20 nm membrane syringe filter

(Whatman) and degassed at 40ºC. A pair of Ag/AgCl electrodes are immersed in the PDMS

chambers. The whole system was placed on a vibration isolated table and surrounded by a

Faraday cage. An Axopatch 200B and digidata 1322A combined system are used to apply the

DC voltage and to measure the current signal through the nanopore. A 10kHz low pass Bessel

filter is applied to filter the current signals, and they are sampled at a rate of 200 kHz. All the

nanopores used in this experiment are characterized by current and voltage curves and have a Current root mean square which indicates noise level less than 10 pA. The data is analyzed by a homemade Matlab program.

Fluidic Chambers

Two fluidic chambers made from Polydimethylsiloxane (PDMS) Cis and Trans were designed to support a nanopore. The ratio of polydimethylsiloxane to hardener is 10:1. After mixing it well, the solution is placed on a heat plate at 70°C for 12 hours. The view of both Cis and Trans chambers is shown in Fig.1(a) and (b) respectively. Cis chamber has a 1 mm opening at the center to bring set the tip above the nanopore surface. Three channels were designed inside the cis chamber, as an inlet and an outlet for the salt solution, and one for an Ag/AgCl electrode. The dimension of the Trans chamber is 2 cm × 2 cm × 1cm and has a 1 mm hole at the center, two channels to flow the electrolyte in and out, and the third channel for an Ag/AgCl electrode to apply a voltage across the chambers. A nanopore chip was inserted between cis and trans and the designated electrolyte solution is used when needed. To measure the ionic current across the nanopore channel, the Ag/AgCl electrodes in each chamber were connected to a current amplifier (Molecular device, Axon 200B). The whole system was enclosed in a home-made Faraday cage to minimize noises caused by electromagnetic radiation. As explained in the nanopore fabrication section, the KOH etching step results in a pyramid-shaped pit. When aligning the chip, the bottom side of the chip should face down touching the trans chamber, and the top of the pyramid face up touching the cis chamber after enclosing both chambers as showing in Fig. 1(b), and the window of the chip should be aligned with both channels from the cis and trans chamber in order to form a perfect tunnel allowing protein freely moving from cis to trans chamber.

11

Protein Sample Preparation

Avidin (67kDa, Thermo Scientific Inc, Pierce Biotechnology, Rockford, Illinois, USA) is dissolved in 1.6 M NaCl salt solution with 20% glycerol at pH 7.5 using Tris buffer to the concentration of 300 nM. Cas9 Nuclease, S. pyogenes (New England Biolabs) is diluted to the concentration of 300 nM using 1.6 M NaCl salt solution with 20% glycerol at pH 7.5.

Nanopore Fabrication

Silicon nitride nanopores used in this work were 9 nm × 7 nm in diameters for Avidin and 25 nm × 22 nm for Cas9. These nanopores were fabricated in free-standing silicon nitride membranes supported by 3 mm × 3 mm silicon substrate chips using the Focus Ion beam sculpting procedure introduced by Dr. Li et.al[63]. Solid-state nanopores are sculpted from a sub-micron hole in free-standing silicon nitride (Si_3N_4) membrane with a high energy noble gas ion beam. The particular process of free-standing Si_3N_4 membrane preparation is discussed here[64]. In general, a 380 µm thick silicon wafer with 275 nm low-pressure chemical vapor deposition (LPCVD) of Si_3N_4 on both sides, is used to fabricate a free Si_3N_4 membrane. Photolithographically designed polymer etch membrane is applied to cover the bottom surface completely and leave an approximately 500 µm Silicon nitride open region on top for etching. Next, a silicon chip is Reactive Ion Etched to remove the silicon nitride now exposed in the windows and trenches by photolithography. Finally, the photoresist is removed from the wafer, which is done by rinsing the wafer in acetone, as well as dipping the wafer in a hot bath of photoresist stripper. The wafer is then placed in a bath of 30% KOH at 90º C to etch pits and trenches through the wafer and to create a reverse pyramid-shaped hollow region with. As an anisotropic etchant, potassium hydroxide does not etch the silicon nitride membrane. Once the membrane is ready, a Focused Ion beam is used to drill a hole through the free-standing silicon nitride membrane. A transmission electron

microscope (TEM) image of the FIB drilled hole is taken. Then the single chip with FIB pore is loaded into the Ion Beam Sculpting apparatus (IBSA). The complete description of the IBSA is discussed here[65]. Briefly, a 3keV He gas ion beam bombarded normally on the FIB drilled hole in the SiN_x membrane. Electrostatic lens systems are applied to focus the ions that pass through the FIB hole on the Channeltron style single ion detector. The mass ion flow that strikes above the FIB hole surface will shrink the top of the hole. The number of ions passing through will demonstrate the size of the hole, small amounts of ions passing means a small area of the pore. Know the initial area of FIB measured from TEM, the beam is deflected away using LabVIEW controlled feedback system when the desired size of a nanopore is achieved. At last, nanopores are annealed at 800℃ for 1 hour in dry nitrogen gas in a tube furnace, and they are imaged under TEM again to measure the final size after closing the procedure[65].
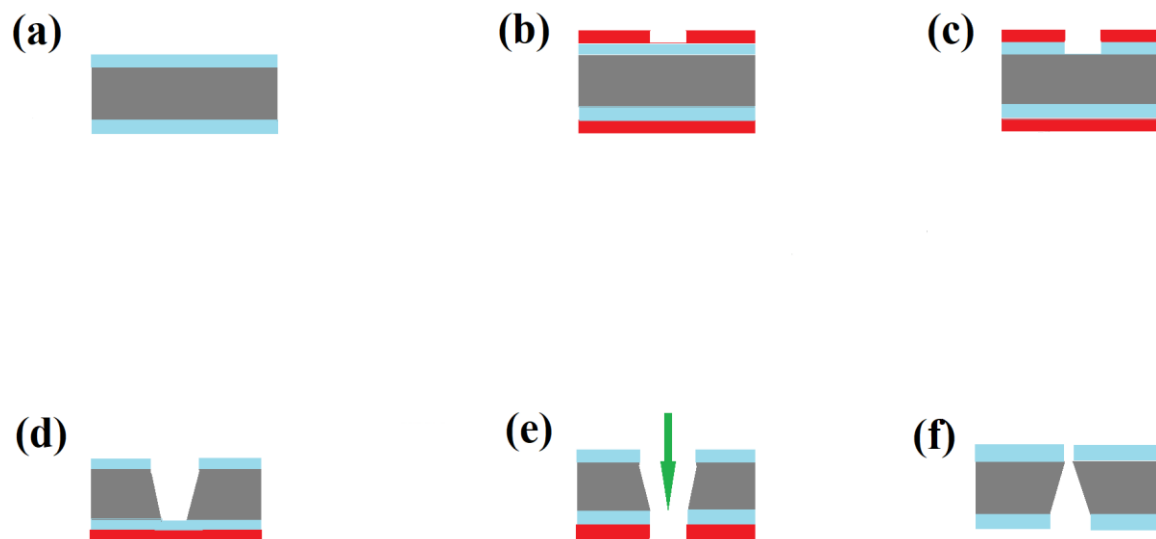
Figure 1.2: Schematics of the Ion Beam Sculpting nanopore fabrication procedure: (a) both sides of the 380 μm thick silicon wafer are coated with a 275 nm thin layer of LPCVD low tensile, silicon nitride. (b) Photo lithographically designed polymer etch mask covers the bottom surface completely and 579 μm silicon nitride region is open for etching. (c) RIE etch of the uncovered SiN_x region on the top surface. (d) KOH wet etch of silicon, gives a 30 μm free-standing SiN_x membrane. (e) 50 keV highly focused Ga^+ ion beam is used to create a 100 nm hole (FIB hole). (f) 3keV energy, broad parallel beam of noble gas ions are bombarded on the free-standing silicon nitride membrane with FIB hole, resulting in a motion of mass from the surface to the hole. Ions passing through the resulting hole are counted by a Channeltron, a single ion counter as a feedback system to control the size of the pore precisely.

Result and Discussion

The close match between the avidin outer dimensions and the pore's inner dimension makes this pair attractive for our goal. The shape of avidin resembles an hourglass with one end slightly bigger than the other, and the shape of the current drop demonstrated in figure 2a appears across all data collected illustrated our assumption. Glycerol is known to reduce protein flexibility, shift protein to a more compact state. Glycerol also prevents protein aggregation and stabilizes the protein in general[20]. We have noticed that the viscosity of the solution significantly impacted Avidin protein translocation time by increasing it generally. At the same voltage(150mv), The

translocation time is 75 microseconds in 1% glycerol and 150 microseconds in 20% glycerol in figure 2b, c, and d. The reasons that voltage of trial 20% glycerol viscosity started at 150mv instead of 30mv like in 1% glycerol are enormous error rates in Gaussian fit and an infrequent number of current drops. For current amplitude, the 1 M NaCl 1% glycerol viscosity has an amplitude of 130 at 150mv, and 1.6 M NaCl 20% glycerol viscosity has an amplitude of 72 at 150mv. Demonstrated in Figures 3a, b, and c. The current amplitude of 20% glycerol solution is smaller and increasing steadily with the voltage increasing compared to the 1% glycerol solution. Our result demonstrated that higher viscosity plays an impactful role in the translocation time of Avidin through the solid-state nanopore.

A similar situation occurs in the case of Cas9, high viscosity increases the translocation duration, and the relationship between current and voltage is always linear in both viscosity solutions. However, unlike the Avidin case, Cas9 protein obeys the ohmic relationship described above which viscosity does not affect the current blockage because of 1 M NaCl 1% glycerol shares almost identical conductivity to 1.6 M NaCl 20% glycerol which is around 80,000 µS/cm. We suspect the reason being the different proportions between the molecule and the nanopore, and the susceptibility of protein structure to salt concentration. In the case of Avidin, a very similar size nanopore (9 nm × 7 nm pore against 7 nm × 6 nm × 5 nm avidin molecule) is employed to slow down the molecule when it gets close to the pore or even to force it to pass the pore in a certain orientation. Good results are found from both concentrations demonstrating the unique hourglass shape of Avidin.

As the reason why higher viscosity's current amplitude is approximately half of the lower viscosity, we suspect that the small nanopore, higher viscosity, and larger voltage might have ripped avidin into two individual molecules each consisting of two subunits since avidin is

15

consist of four identical subunits. Also, higher salt concentration contributes to the change of

protein structure due to electrostatic interactions. Cas9 does not show the same pattern as avidin

because a relatively larger pore is employed (25 nm × 22 nm pore against 15 nm × 20 nm × 9 nm

Cas9 molecule) and its susceptibility to change structure due to salt concentration. Moreover,

different choices of salt could also be a factor. Normally, potassium chloride is widely used in

solid-state nanopore especially in SiN. The baseline current of this work at any voltage is

sometimes lower than potassium chloride counterparts.

Figure 5 and 6 demonstrate that our Cas9 data share similarities with the oblate profile compared

to Jared Houghtaling, et al's work, our Cas9 current signatures fits the description of

oblate/prolate protein's signature with a deeper blockage at around 600 pA representing oblate

conformation and a lower blockage at around 850 pA representing prolate conformation. Avidin

signatures in figure 7 show that avidin fits the category of general spherical protein signatures for

having one type of constant current blockage around 600 pA, and figure 7b shows that it meets

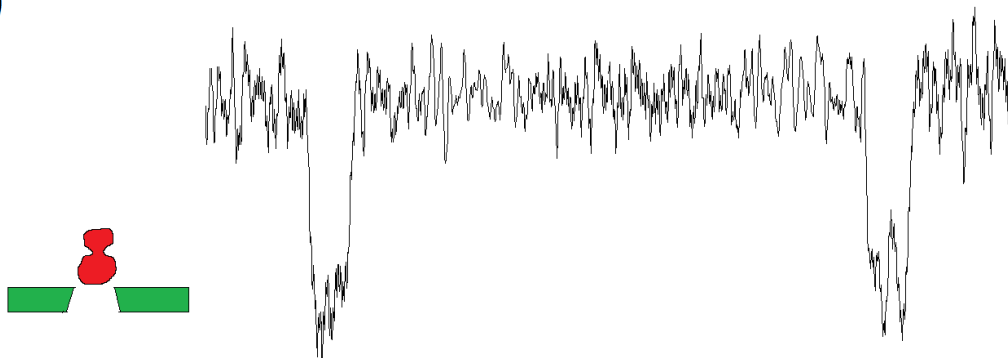the hourglass shape described at figure 2b.

(a)

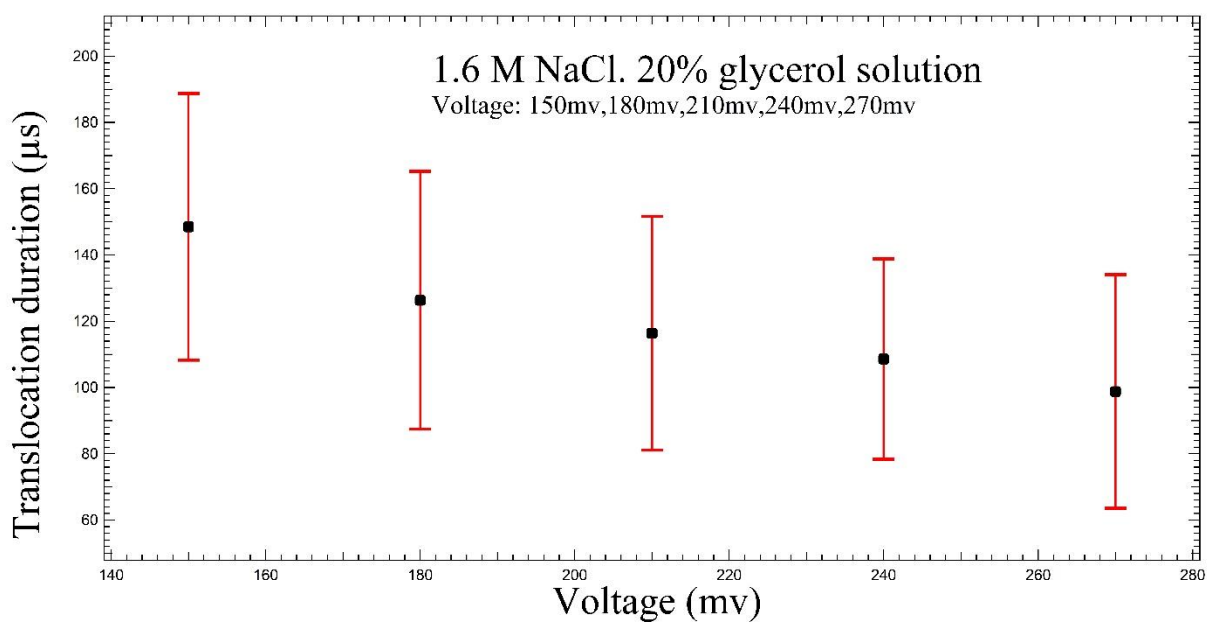Figure 2(a): examples of Avidin's current blockage drops.

Figure 2(b): Translocation duration trend from 150 mv to 270 mv in 1.6 M 20% glycerol NaCl solution at 7.5 pH.
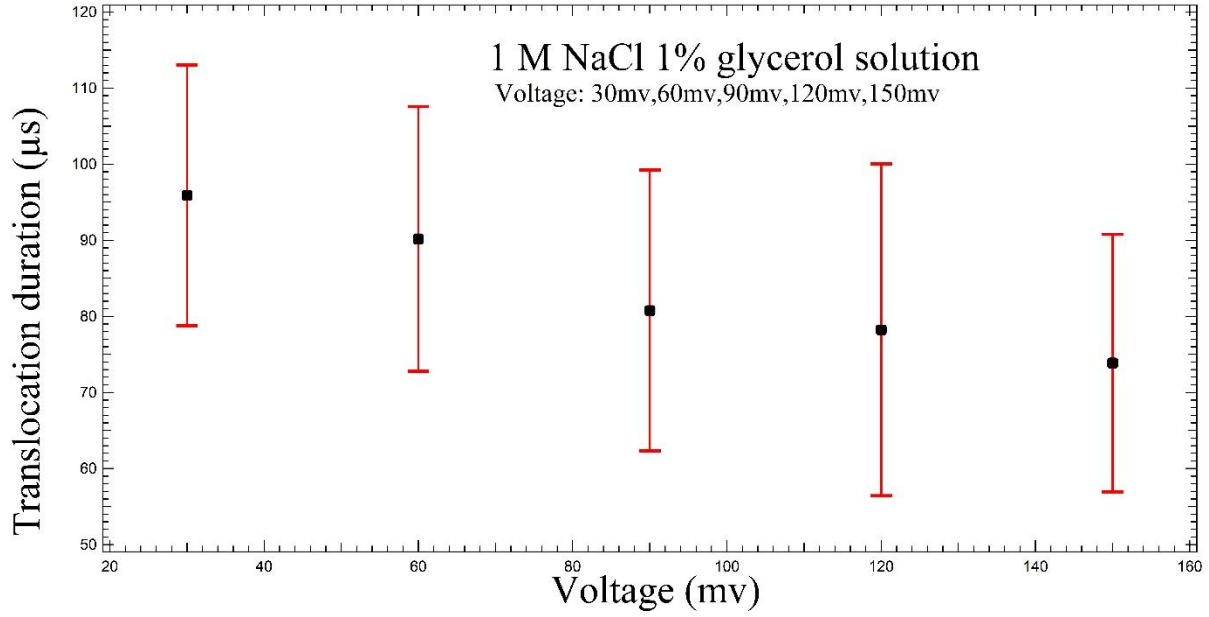
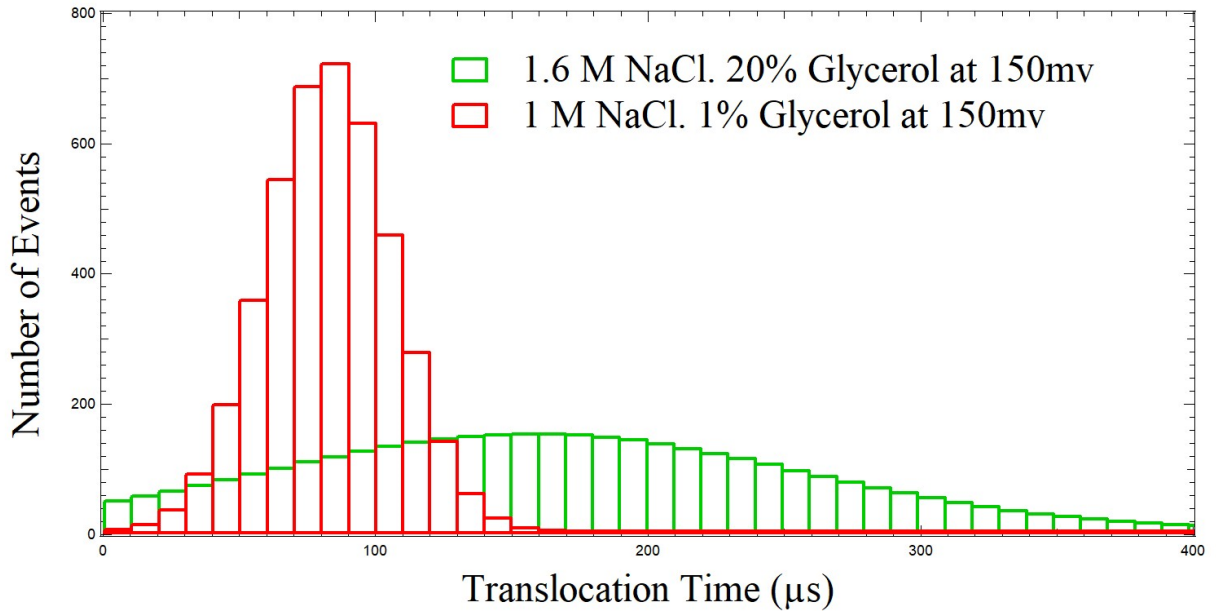Figure 2(c): Translocation duration trend from 30 mv to 150 mv in 1 M 1% glycerol NaCl solution at 7.5 pH.

Figure 2(d): The Gaussian fit of Translocation time at 150 mv for two different viscosity solutions.
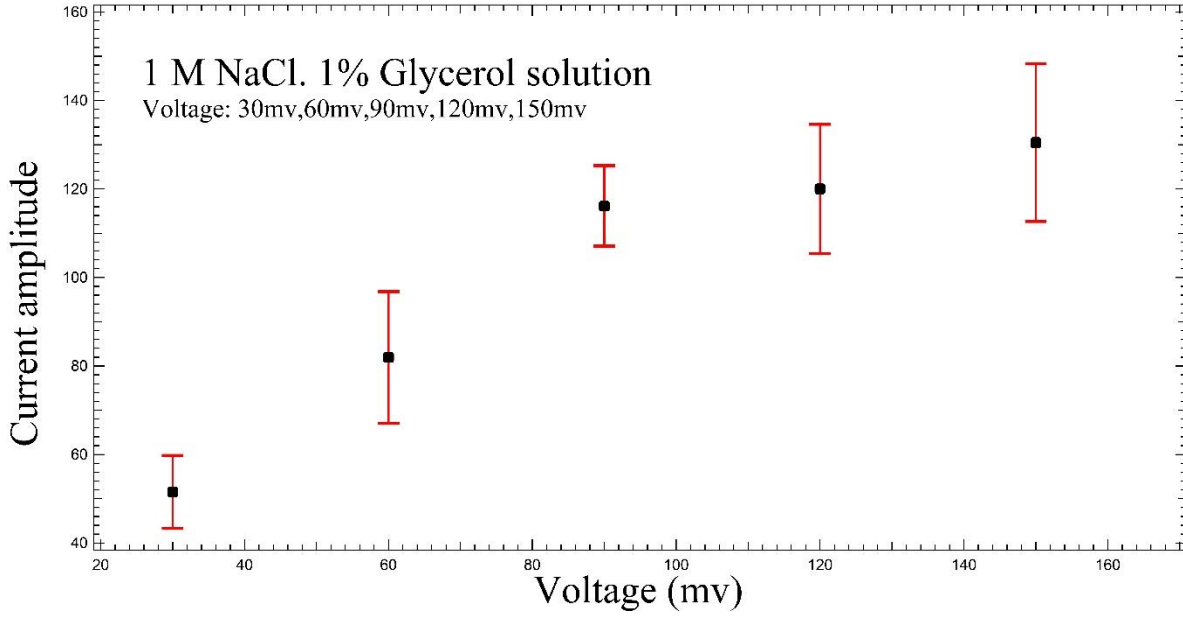
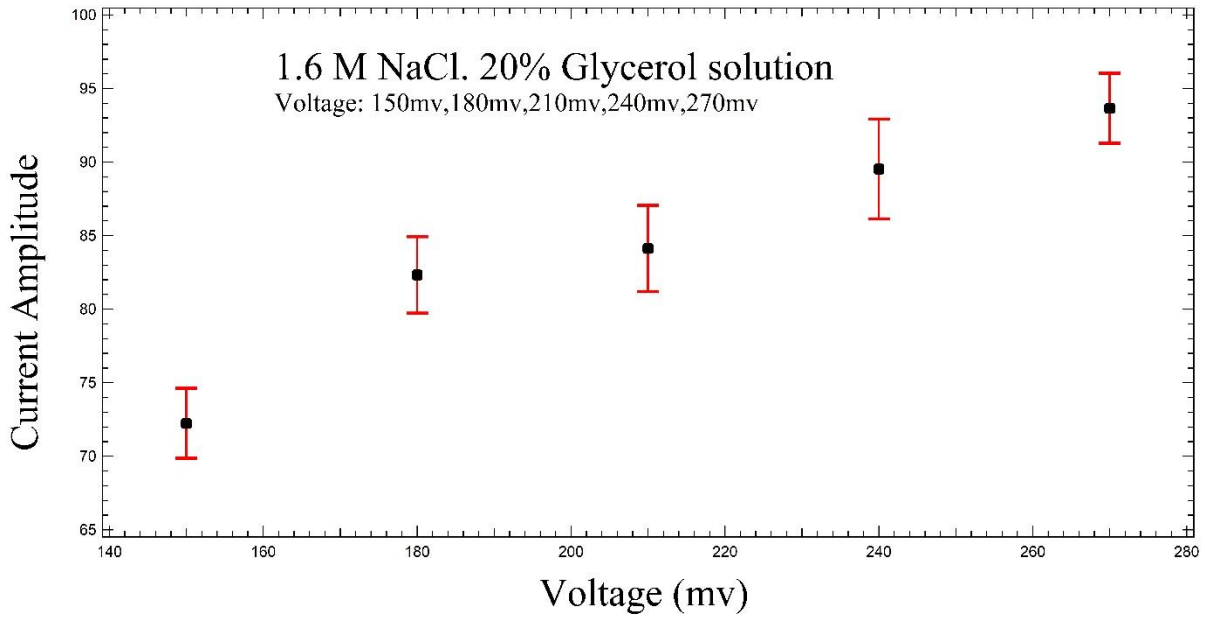Figure 3(a): Current amplitude tendency from 30 mv to 150 mv in 1M NaCl 1% glycerol solution at pH 7.5.

Figure 3(b): Current amplitude tendency from 150mv to 270mv in 1.6 M NaCl 20% glycerol at pH 7.5.
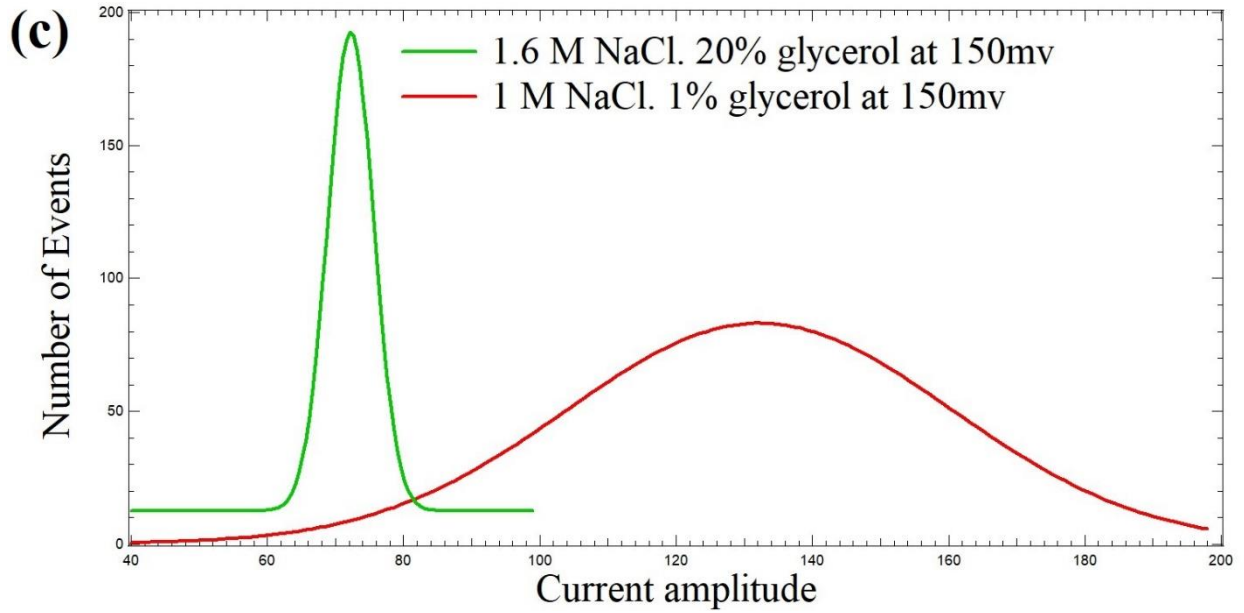
(c)

Figure 3(c): The Gaussian fit of 1.6 M NaCl 20% glycerol and 1 M NaCl 1% glycerol at 150 mv at pH 7.5.
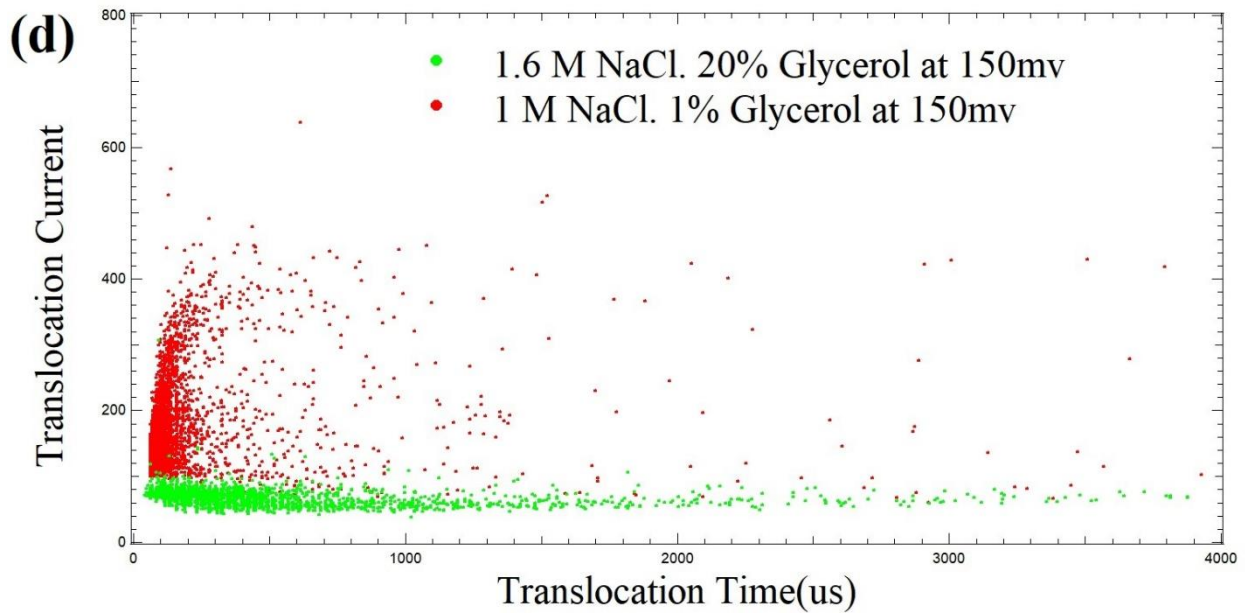
(d)

Figure 3(d): Scatter plot of avidin in two different concentrations.
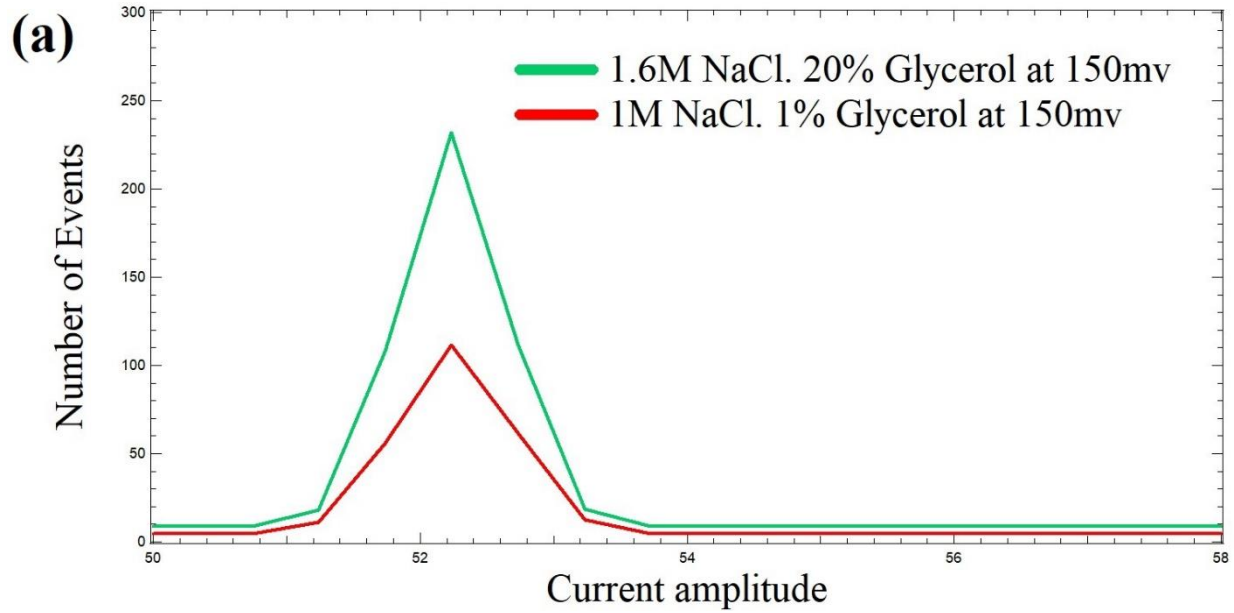
20

Figure 4(a): The Gaussian fit of the current amplitude histogram of Cas9 in two different concentration solutions.
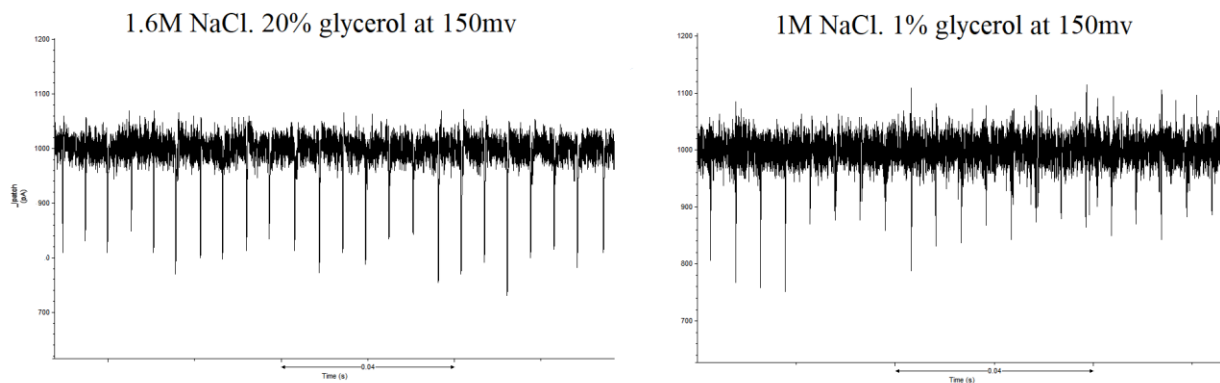
(b)

Figure 4(b): Current trace of Cas9 at 150mv in 1.6M NaCl 20% glycerol and 1M NaCl 1% glycerol relatively.
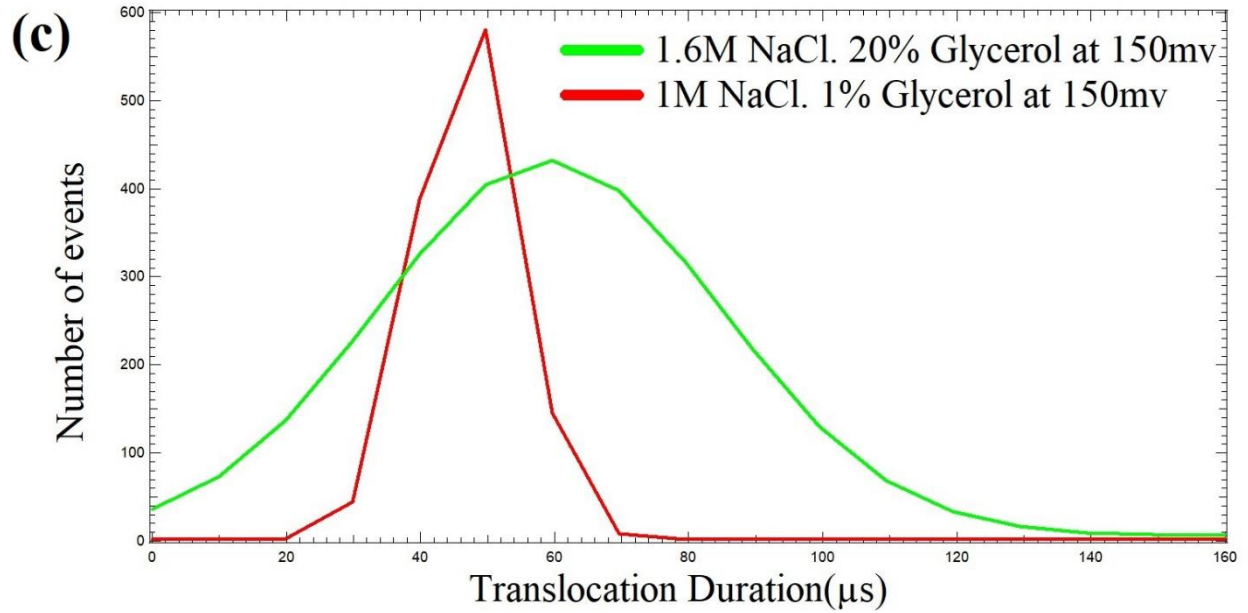
Figure 4(c): The Gaussian fit of the Translocation Duration histogram of Cas9 in two different concentration solutions.
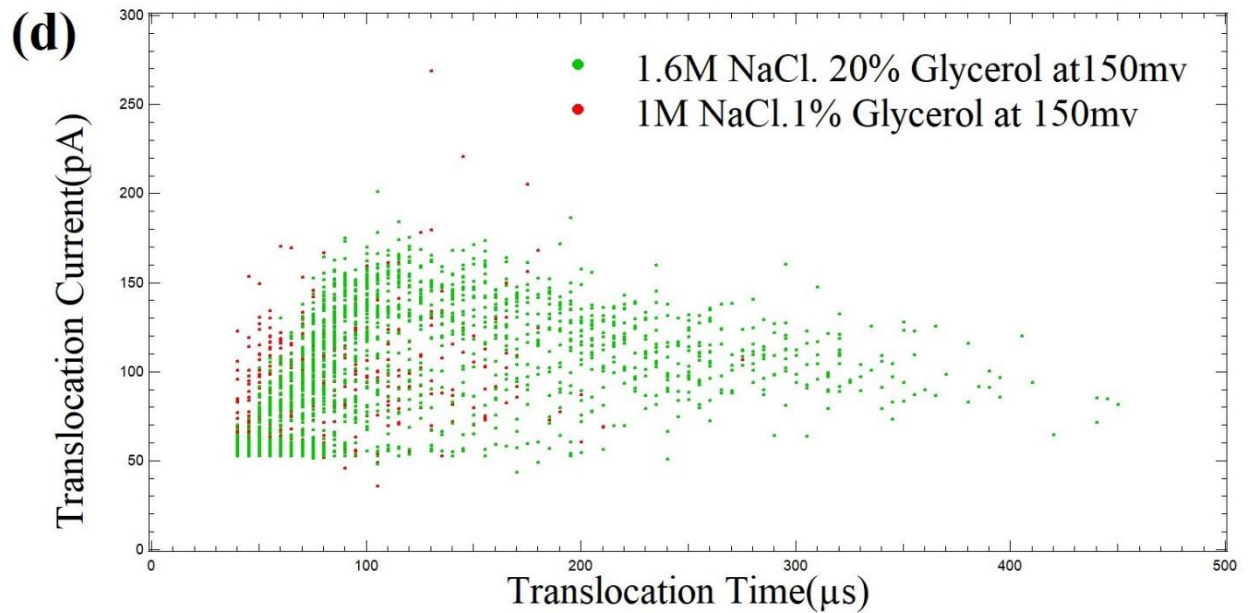

Figure 4(d): Scatter plot of Cas9 in two solutions both at 150mv.
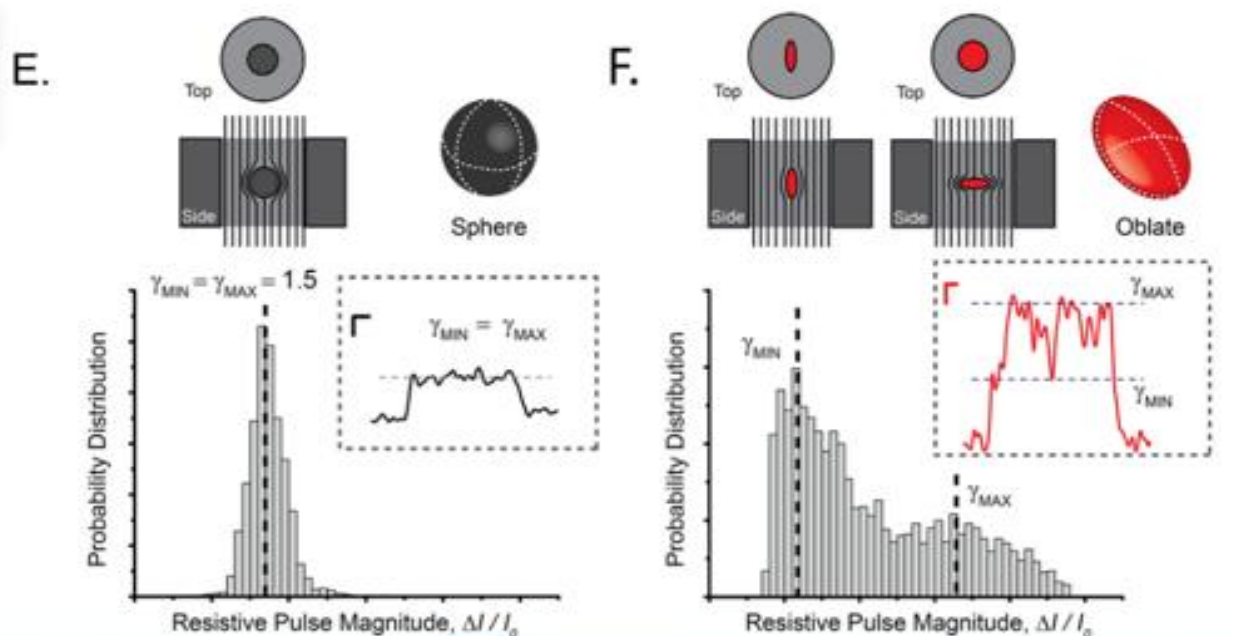
Figure 5. Maximum and minimum blockade values corresponding to electrical shape factors. Houghtaling, Jared, et al. "Estimation of Shape, Volume, and Dipole Moment of Individual Proteins Freely Transiting a Synthetic Nanopore." *ACS Nano*, vol. 13, no. 5, 2019, pp. 5231–5242., doi:10.1021/acsnano.8b09555
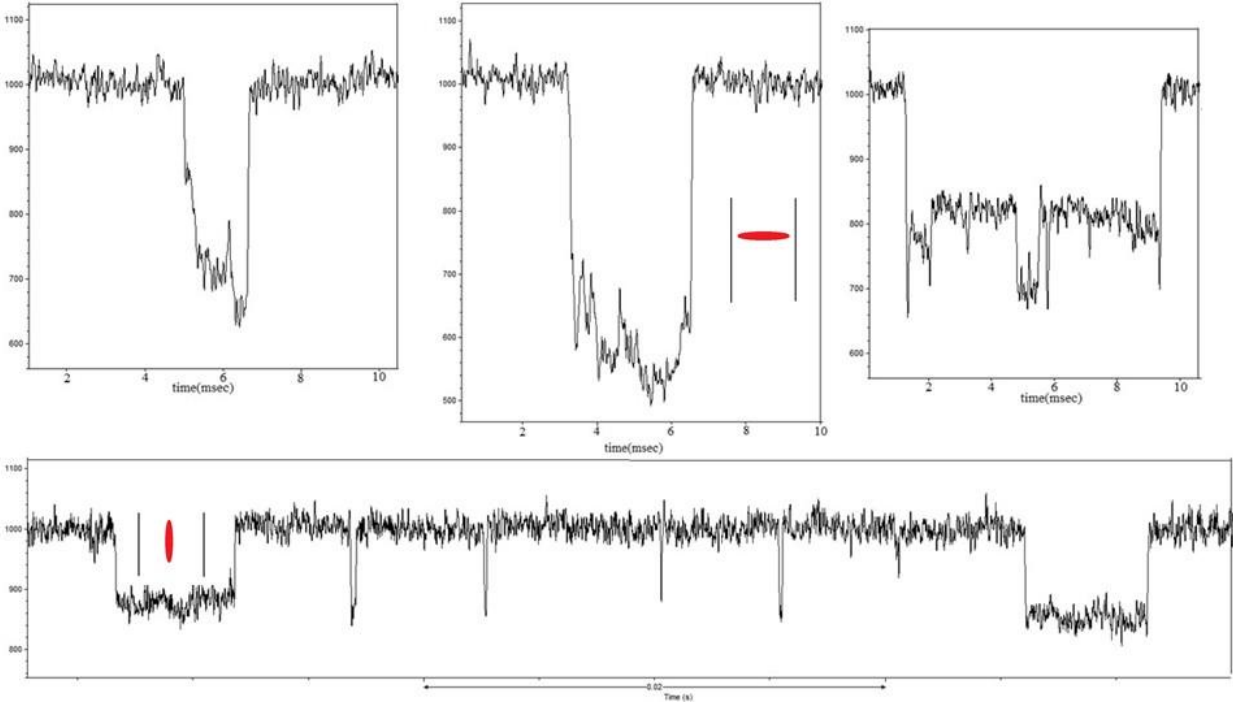
Figure 6. Cas9's current signature.
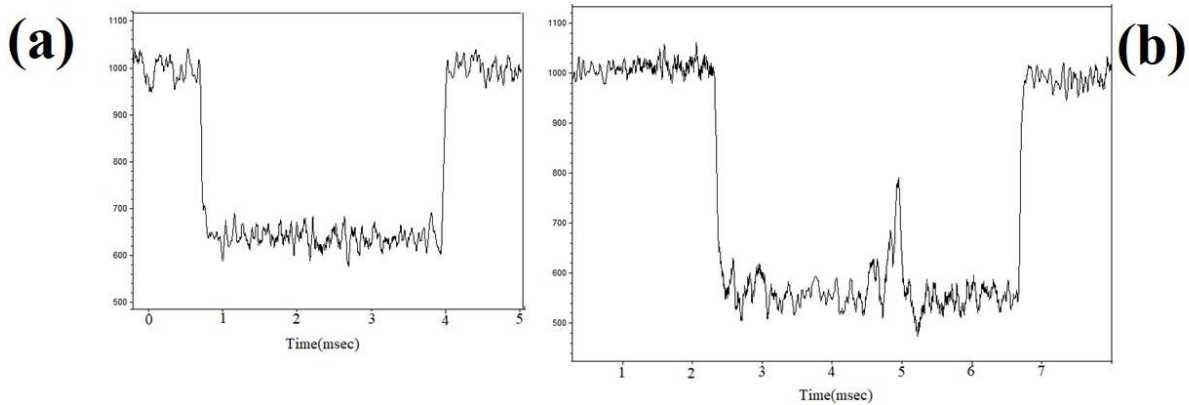
Figure 7. Current signatures of Avidin.

Conclusion

By using equation 3, we calculated the volume of avidin to be 230 nm^3. It is a reasonable value compare to Dr. Yusko et al's 161 nm^3 of streptavidin's volume since Streptavidin and Avidin are considered spherical shape with shape factor ($\gamma=1.5$)[38]. However, the shape factor for a non-spherical protein such as Cas9 depends on the conformation when it translocates through the nanopore. The current amplitude of avidin demonstrates similar amplitude distribution patterns

24

compare to Streptavidin and other spherical proteins which is the one peak gaussian fit. A two peaks amplitude distribution pattern is expected for Cas9. However, due to the uncontrollable rotation and less comprehensive data, a single peak pattern is generated. The result from both Avidin and Cas9 proteins demonstrates that the translocation of protein molecules is similar to the translocation of DNA molecules. They both obey the ohmic behavior in the ionic solution passing through the nanopore. The current trace is distinct when a long DNA chain passing through the nanopore, and it is easier to tell if a protein is attached to the DNA chain since the thickness of DNA remains constant as a cylindrical shape. Individual protein molecule usually has an asymmetric shape, and they are constantly spinning in an ionic solution maintaining a hydrodynamic radius, therefore, harder to detect the shape of it. That is the motivation behind using the pore that has a similar diameter to the protein. Nevertheless, the natural flaw of this using small pore is also obvious, some protein molecules will generate a blockage signal when hit the surface of the membrane and bounce back, therefore, slightly mislead the data collection. Inspiringly, we share some similar result with Waduge's result on the estimation of the sizes and intrinsic flexibilities of proteins as they slowly squeezed through synthetic nanopores with diameters only slightly larger than the proteins themselves[36], and this confirms that solid-state nanopore has the potential to detect protein conformational change and rigidity. We believe that this study will help solid-state nanopore to become a valuable sensor on protein conformation and size detection. Proteins are more susceptible to outside factors such as pH, salt concentration and nanopore size than DNA molecules, an example would be that high concentration salt will interfere with the electrostatic interaction of protein in solution hence break the bond of protein molecules.

In the future, more comprehensive research will be conducted on both Avidin and Cas9 to demonstrate the specific role of each independent variable plays during the translocation. Moreover, potassium chloride will also be used to compare how different salt solutions affect the protein in a solid-state nanopore. More experiments will be performed to confirm the specificity of protein interaction with the solid-state nanopore. The ease of approach of our Avidin and Cas9 detection scheme over the other techniques makes nanopore sensing of different biomolecules a promising platform for disease detection and diagnostics. Indeed, we visualize the massive use of such nanopore detection for the fast detection and identification of More biomolecules such as dsDNA, ssDNA, large and small proteins.

Reference

1. Tan, Yih Horng, et al. "Characterization of Protein Immobilization on Nanoporous Gold Using Atomic Force Microscopy and Scanning Electron Microscopy." *Nanoscale*, vol. 3, no. 8, 2011, p. 3395., doi:10.1039/c1nr10427f.

2. Haas, Elisha. "The Study of Protein Folding and Dynamics by Determination of Intramolecular Distance Distributions and Their Fluctuations Using Ensemble and Single-Molecule FRET Measurements." *ChemPhysChem*, vol. 6, no. 5, 2005, pp. 858–870., doi:10.1002/cphc.200400617.

3. Eggertson, Michael J., and Douglas B. Craig. "Laser-Induced Fluorescence Detector for Liquid Chromatography: Applications to Protein Analysis." *Biomedical Chromatography*, vol. 14, no. 3, 2000, pp. 156–159., doi:10.1002/1099-0801(200005)14:3<156::aid-bmc942>3.0.co;2-x.

4. Gosse, Charlie, and Vincent Croquette. "Magnetic Tweezers: Micromanipulation and Force Measurement at the Molecular Level." *Biophysical Journal*, vol. 82, no. 6, 2002, pp. 3314–3329., doi:10.1016/s0006-3495(02)75672-5.

5. Neuman, Keir C, and Attila Nagy. "Single-Molecule Force Spectroscopy: Optical Tweezers, Magnetic Tweezers, and Atomic Force Microscopy." *Nature Methods*, vol. 5, no. 6, 2008, pp. 491–505., doi:10.1038/nmeth.1218.

6. Harper, James D., et al. "Observation of Metastable Aβ Amyloid Protofibrils by Atomic Force Microscopy." *Chemistry & Biology*, vol. 4, no. 2, 1997, pp. 119–125., doi:10.1016/s1074-5521(97)90255-6.

7. Song, L., et al. "Structure of Staphylococcal Alpha -Hemolysin, a Heptameric Transmembrane Pore." *Science*, vol. 274, no. 5294, 1996, pp. 1859–1865., doi:10.1126/science.274.5294.1859.

8. Faller, M. "The Structure of a Mycobacterial Outer-Membrane Channel." *Science*, vol. 303, no. 5661, 2004, pp. 1189–1192., doi:10.1126/science.1094114.

9. Butler, T. Z., et al. "Single-Molecule DNA Detection with an Engineered MspA Protein Nanopore." *Proceedings of the National Academy of Sciences*, vol. 105, no. 52, 2008, pp. 20647–20652., doi:10.1073/pnas.0807514106.

10. Fu, Chi-Yu, and Peter E. Prevelige. "In Vitro Incorporation of the Phage Phi29 Connector Complex." *Virology*, vol. 394, no. 1, 2009, pp. 149–153., doi:10.1016/j.virol.2009.08.016.

11. Simpson, A.a., et al. "Structure of the Bacteriophage phi29 Head-Tail Connector Protein." Sept. 2001, doi:10.2210/pdb1ijg/pdb.

12. Guo, Yinyin, et al. "Construction and 3-D Computer Modeling of Connector Arrays with Tetragonal to Decagonal Transition Induced by PRNA of phi29 DNA-Packaging Motor." *Journal of Nanoscience and Nanotechnology*, vol. 5, no. 6, Jan. 2005, pp. 856–863., doi:10.1166/jnn.2005.143.

13. Wendell, David, et al. "Translocation of Double-Stranded DNA through Membrane-Adapted phi29 Motor Protein Nanopores." *Nature Nanotechnology*, vol. 4, no. 11, 2009, pp. 765–772., doi:10.1038/nnano.2009.259.

14. Jing, Peng, et al. "Robust Properties of Membrane-Embedded Connector Channel of Bacterial Virus phi29 DNA Packaging Motor." *Molecular BioSystems*, vol. 6, no. 10, 2010, p. 1844., doi:10.1039/c003010d.

15. Haque, Farzin, et al. "Real-Time Sensing and Discrimination of Single Chemicals Using the Channel of Phi29 DNA Packaging Nanomotor." *ACS Nano*, vol. 6, no. 4, Sept. 2012, pp. 3251–3261., doi:10.1021/nn3001615.

16. Hout, Michiel Van Den, et al. "Controlling Nanopore Size, Shape and Stability." *Nanotechnology*, vol. 21, no. 11, 2010, p. 115304., doi:10.1088/0957-4484/21/11/115304.

17. Wanunu, Meni, et al. "Nanopore Analysis of Individual RNA/Antibiotic Complexes." *ACS Nano*, vol. 5, no. 12, 2011, pp. 9345–9353., doi:10.1021/nn203764j.

18. Li, Jiali, et al. "Ion-Beam Sculpting at Nanometre Length Scales." *Nature*, vol. 412, no. 6843, 2001, pp. 166–169., doi:10.1038/35084037.

19. Dekker C. Nature Nanotechnology. 2007;2:209.

20. Schadt, E. E., et al. "A Window into Third-Generation Sequencing." *Human Molecular Genetics*, vol. 19, no. R2, 2010, doi:10.1093/hmg/ddq416.

21. Liu, Lin, et al. "Comparison of Next-Generation Sequencing Systems." *Journal of Biomedicine and Biotechnology*, vol. 2012, 2012, pp. 1–11., doi:10.1155/2012/251364.

22. Wang, Yue, et al. "The Evolution of Nanopore Sequencing." *Frontiers in Genetics*, vol. 5, July 2015, doi:10.3389/fgene.2014.00449.

23. Branton, Daniel, et al. "The Potential and Challenges of Nanopore Sequencing." *Nature Biotechnology*, vol. 26, no. 10, 2008, pp. 1146–1153., doi:10.1038/nbt.1495.

24. Ding, Fangyuan, et al. "Single-Molecule Mechanical Identification and Sequencing." *Nature Methods*, vol. 9, no. 4, Nov. 2012, pp. 367–372., doi:10.1038/nmeth.1925.

25. Cheng, Peng, et al. "Progress toward the Application of Molecular Force Spectroscopy to DNA Sequencing." *Electrophoresis*, vol. 33, no. 23, 2012, pp. 3497–3505., doi:10.1002/elps.201200351.

26. Treffer, Regina, et al. "Distinction of Nucleobases – a Tip-Enhanced Raman Approach." *Beilstein Journal of Nanotechnology*, vol. 2, 2011, pp. 628–637., doi:10.3762/bjnano.2.66.

27. Sha, Jingjie, et al. "Identification of Spherical and Nonspherical Proteins by a Solid-State Nanopore." *Analytical Chemistry*, vol. 90, no. 23, 2018, pp. 13826–13831., doi:10.1021/acs.analchem.8b04136.

28. Fologea, D., Ledden, B., McNabb, D.S.& Li, J. "Electrical Characterization of Protein Molecules by a Solid-State Nanopore." *Applied Physics Letters*, vol. 91, no. 5, 2007, p. 053901., doi:10.1063/1.2767206.

29. Li, Jiali, et al. "DNA Molecules and Configurations in a Solid-State Nanopore Microscope." *Nature Materials*, vol. 2, no. 9, 2003, pp. 611–615., doi:10.1038/nmat965.

30. Heng, Jiunn B., et al. "Sizing DNA Using a Nanometer-Diameter Pore." *Biophysical Journal*, vol. 87, no. 4, 2004, pp. 2905–2911., doi:10.1529/biophysj.104.041814.

31. Fologea, Daniel, et al. "Detecting Single-Stranded DNA with a Solid-State Nanopore." *Nano Letters*, vol. 5, no. 10, 2005, pp. 1905–1909., doi:10.1021/nl051199m.

32. Storm, A. J., Chen, J. H., Zandbergen, H. W., Dekker, C. "Translocation of Double-Strand DNA through a Silicon Oxide Nanopore." *Physical Review E*, vol. 71, no. 5, 2005, doi:10.1103/physreve.71.051903.

33. Madampage, Claudia Avis, et al. "Nanopore Detection of Antibody Prion Interactions." *Analytical Biochemistry*, vol. 396, no. 1, 2010, pp. 36–41., doi:10.1016/j.ab.2009.08.028.

34. Yusko, Erik C., et al. "Controlling Protein Translocation through Nanopores with Bio-Inspired Fluid Walls." *Nature Nanotechnology*, vol. 6, no. 4, 2011, pp. 253–260., doi:10.1038/nnano.2011.12.

35. Liu, Nannan, et al. "Nanopore-Based Analysis of Biochemical Species." *Microchimica Acta*, vol. 183, no. 3, 2015, pp. 955–963., doi:10.1007/s00604-015-1560-2.

36. Waduge, Pradeep, et al. "Nanopore-Based Measurements of Protein Size, Fluctuations, and Conformational Changes." *ACS Nano*, vol. 11, no. 6, Sept. 2017, pp. 5706–5716., doi:10.1021/acsnano.7b01212.

37. Soni, Gautam V., and Cees Dekker. "Detection of Nucleosomal Substructures Using Solid-State Nanopores." *Nano Letters*, vol. 12, no. 6, Aug. 2012, pp. 3180–3186., doi:10.1021/nl301163m.

38. Yusko, Erik C., et al. "Real-Time Shape Approximation and Fingerprinting of Single Proteins Using a Nanopore." *Nature Nanotechnology*, vol. 12, no. 4, 2016, pp. 360–367., doi:10.1038/nnano.2016.267.

39. Cornell, B. A., et al. "A Biosensor That Uses Ion-Channel Switches." *Nature*, vol. 387, no. 6633, 1997, pp. 580–583., doi:10.1038/42432.

40. Coulter, Wallace H. Means for counting particles suspended in a fluid. United States Patent Office. Patented am 20, 1953 (1953).

41. Fologea, Daniel, et al. "Slowing DNA Translocation in a Solid-State Nanopore." *Nano Letters*, vol. 5, no. 9, 2005, pp. 1734–1737., doi:10.1021/nl051063o.

42. Han, Anpan, et al. "Label-Free Detection of Single Protein Molecules and Protein−Protein Interactions Using Synthetic Nanopores." *Analytical Chemistry*, vol. 80, no. 12, 2008, pp. 4651–4658., doi:10.1021/ac7025207..

43. Yusko, Erik C., et al. "Controlling Protein Translocation through Nanopores with Bio-Inspired Fluid Walls." *Nature Nanotechnology*, vol. 6, no. 4, 2011, pp. 253–260., doi:10.1038/nnano.2011.12.

44. Houghtaling, Jared, et al. "Estimation of Shape, Volume, and Dipole Moment of Individual Proteins Freely Transiting a Synthetic Nanopore." *ACS Nano*, vol. 13, no. 5, 2019, pp. 5231–5242., doi:10.1021/acsnano.8b09555.

45. Kaur, Harpreet, et al. "Estimating RNA Polymerase Protein Binding Sites on λ DNA Using Solid-State Nanopores." *ACS Sensors*, vol. 4, no. 1, 2018, pp. 100–109., doi:10.1021/acssensors.8b00976

46. Taniguchi, Masateru. "Selective Multidetection Using Nanopores." *Analytical Chemistry*, vol. 87, no. 1, 2014, pp. 188–199., doi:10.1021/ac504186m.

47. Haywood, Daniel G., et al. "Electroosmotic Flow in Nanofluidic Channels." *Analytical Chemistry*, vol. 86, no. 22, Mar. 2014, pp. 11174–11180., doi:10.1021/ac502596m.

48. Haque, Farzin, et al. "Solid-State and Biological Nanopore for Real-Time Sensing of Single Chemical and Sequencing of DNA." *Nano Today*, vol. 8, no. 1, 2013, pp. 56–74., doi:10.1016/j.nantod.2012.12.008.

49. Si, Wei, and Aleksei Aksimentiev. "Nanopore Sensing of Protein Folding." *ACS Nano*, vol. 11, no. 7, 2017, pp. 7091–7100., doi:10.1021/acsnano.7b02718.

50. Kato, Yuta, et al. "Gate-Voltage-Controlled Threading DNA into Transistor Nanopores." *The Journal of Physical Chemistry B*, vol. 122, no. 2, May 2017, pp. 827–833., doi:10.1021/acs.jpcb.7b06932.

51. Oukhaled, Abdelghani, et al. "Dynamics of Completely Unfolded and Native Proteins through Solid-State Nanopores as a Function of Electric Driving Force." *ACS Nano*, vol. 5, no. 5, 2011, pp. 3628–3638., doi:10.1021/nn1034795.

52. Yusko, Erik C., et al. "Real-Time Shape Approximation and Fingerprinting of Single Proteins Using a Nanopore." *Nature Nanotechnology*, vol. 12, no. 4, 2016, pp. 360–367., doi:10.1038/nnano.2016.267.

53. Lu, Bo, et al. "Protein Motion and Configurations in a Form-Fitting Nanopore: Avidin in ClyA." *Biophysical Journal*, vol. 115, no. 5, 2018, pp. 801–808., doi:10.1016/j.bpj.2018.07.024.

54. Lam, Michelle H., et al. "Entropic Trapping of DNA with a Nanofiltered Nanopore." *ACS Applied Nano Materials*, 2019, doi:10.1021/acsanm.9b00606.

55. Tang, Zifan, et al. "Fabrications, Applications and Challenges of Solid-State Nanopores: A Mini-Review." *Nanomaterials and Nanotechnology*, vol. 6, 2016, p. 35., doi:10.5772/64015.

56. Hytönen, Vesa P, et al. *BMC Biotechnology*, vol. 5, no. 1, 2005, p. 28., doi:10.1186/1472-6750-5-28.

57. Green, N.M. Avidin. *Adv. Protein Chem.* 29, 85-133 (1975).

58. Bruch, Richard C. & White, H.B.I. "Compositional and Structural Heterogeneity of Avidin Glycopeptides." *Biochemistry*, vol. 21, no. 21, 1982, pp. 5334–5341., doi:10.1021/bi00264a033.

59. Livnah, O., Bayer, E.A., Wilchek, M. & Sussman, J.L. "Three-Dimensional Structures of Avidin and the Avidin-Biotin Complex." *Proceedings of the National Academy of Sciences*, vol. 90, no. 11, 1993, pp. 5076–5080., doi:10.1073/pnas.90.11.5076.

60. Pugliese, L., Malcovati, M., Coda, A. & Bolognesi, M. "Crystal Structure of Apo-Avidin from Hen Egg-White." *Journal of Molecular Biology*, vol. 235, no. 1, 1994, pp. 42–46., doi:10.1016/s0022-2836(05)80010-5.

61. Jinek, M., et al. "Structures of Cas9 Endonucleases Reveal RNA-Mediated Conformational Activation." *Science*, vol. 343, no. 6176, June 2014, pp. 1247997–1247997., doi:10.1126/science.1247997.

62. Sternberg, Samuel H., et al. "DNA Interrogation by the CRISPR RNA-Guided Endonuclease Cas9." *Nature*, vol. 507, no. 7490, 2014, pp. 62–67., doi:10.1038/nature13011.

63. Vagenende, Vincent, et al. "Mechanisms of Protein Stabilization and Prevention of Protein Aggregation by Glycerol." *Biochemistry*, vol. 48, no. 46, 2009, pp. 11084–11096., doi:10.1021/bi900649t.

64. Kato, Yuta, et al. "Gate-Voltage-Controlled Threading DNA into Transistor Nanopores." *The Journal of Physical Chemistry B*, vol. 122, no. 2, May 2017, pp. 827–833., doi:10.1021/acs.jpcb.7b06932.

65. Li, Jiali, et al. "Ion-Beam Sculpting at Nanometre Length Scales." *Nature*, vol. 412, no. 6843, 2001, pp. 166–169., doi:10.1038/35084037.

66. Ladden, Bradley Thomas. "Fabrication of Solid States Nanopores Using Feedback Controlled Ion Beam Sculpting Techniques." Ph.D. thesis, University of Arkansas (2004).

67. Hsu, Wei-Lun, and Hirofumi Daiguji. "Manipulation of Protein Translocation through Nanopores by Flow Field Control and Application to Nanopore Sensors." *Analytical Chemistry*, vol. 88, no. 18, Sept. 2016, pp. 9251–9258., doi:10.1021/acs.analchem.6b02513.

68. Merchant, Chris. "DNA Translocation Through Graphene Nanopores." *Biophysical Journal*, vol. 100, no. 3, 2011, doi:10.1016/j.bpj.2010.12.3046.

69. Wells, David B., et al. "Assessing Graphene Nanopores for Sequencing DNA." *Nano Letters*, vol. 12, no. 8, 2012, pp. 4117–4123., doi:10.1021/nl301655d.

70. Venkatesan, Bala Murali, et al. "Stacked Graphene-Al2O3 Nanopore Sensors for Sensitive Detection of DNA and DNA–Protein Complexes." *ACS Nano*, vol. 6, no. 1, 2011, pp. 441–450., doi:10.1021/nn203769e.

71. Prasongkit, Jariyanee, et al. "Transverse Conductance of DNA Nucleotides in a Graphene Nanogap from First Principles." *Nano Letters*, vol. 11, no. 5, Nov. 2011, pp. 1941–1945., doi:10.1021/nl200147x.

72. Houghtaling, Jared, et al. "Estimation of Shape, Volume, and Dipole Moment of Individual Proteins Freely Transiting a Synthetic Nanopore." *ACS Nano*, vol. 13, no. 5, 2019, pp. 5231–5242., doi:10.1021/acsnano.8b09555.